

Plasmonic Band Structure Controls Single Molecule Fluorescence

Lutz Langguth, Deep Punj, Jerome Wenger, and A. Femius Koenderink

ACS Nano, **Just Accepted Manuscript** • DOI: 10.1021/nn4033008 • Publication Date (Web): 10 Sep 2013

Downloaded from <http://pubs.acs.org> on September 11, 2013

Just Accepted

“Just Accepted” manuscripts have been peer-reviewed and accepted for publication. They are posted online prior to technical editing, formatting for publication and author proofing. The American Chemical Society provides “Just Accepted” as a free service to the research community to expedite the dissemination of scientific material as soon as possible after acceptance. “Just Accepted” manuscripts appear in full in PDF format accompanied by an HTML abstract. “Just Accepted” manuscripts have been fully peer reviewed, but should not be considered the official version of record. They are accessible to all readers and citable by the Digital Object Identifier (DOI®). “Just Accepted” is an optional service offered to authors. Therefore, the “Just Accepted” Web site may not include all articles that will be published in the journal. After a manuscript is technically edited and formatted, it will be removed from the “Just Accepted” Web site and published as an ASAP article. Note that technical editing may introduce minor changes to the manuscript text and/or graphics which could affect content, and all legal disclaimers and ethical guidelines that apply to the journal pertain. ACS cannot be held responsible for errors or consequences arising from the use of information contained in these “Just Accepted” manuscripts.



Plasmonic Band Structure Controls Single Molecule Fluorescence

Lutz Langguth,^{*,†} Deep Punj,[‡] Jérôme Wenger,[‡] and A. Femius Koenderink[†]

Center for Nanophotonics, FOM Institute for Atomic and Molecular Physics (AMOLF), Science Park 104, 1098 XG Amsterdam, The Netherlands, and CNRS, Aix-Marseille Université, Ecole Centrale Marseille, Institut Fresnel, Campus de St Jérôme, 13397 Marseille, France

E-mail: L.Langguth@amolf.nl

Abstract

Plasmonics and photonic crystals are two complementary approaches to tailor single emitter fluorescence, using strong local field enhancements near metals on one hand, and spatially extended photonic band structure effects on the other hand. Here, we explore the emergence of spontaneous emission control by finite-sized hexagonal arrays of nanoapertures milled in gold film. We demonstrate that already small lattices enable highly directional and enhanced emission from single fluorescent molecules in the central aperture. Even for clusters just four unit cells across, the directionality is set by the plasmonic crystal band structure, as confirmed by full-wave numerical simulations. This realization of plasmonic phase array antennas driven by single quantum emitters opens a flexible toolbox to engineer fluorescence and its detection.

^{*}To whom correspondence should be addressed

[†]Center for Nanophotonics, FOM Institute for Atomic and Molecular Physics (AMOLF), Science Park 104, 1098 XG Amsterdam, The Netherlands

[‡]CNRS, Aix-Marseille Université, Ecole Centrale Marseille, Institut Fresnel, Campus de St Jérôme, 13397 Marseille, France

1
2
3 **Keywords:** nanoantenna, plasmonics, plasmonic crystal, nanoaperture, fluorescence enhance-
4 ment, Bloch mode
5
6

7
8 Achieving a complete manipulation of the generally weak optical signal from a single quantum
9 emitter is a key objective in nanophotonics. To this end, two major routes have been investigated:
10 plasmonic metal nanostructures¹⁻¹¹ and dielectric photonic crystals.¹²⁻²¹ Both routes have demon-
11 strated breakthrough results in tailoring the photoluminescence intensity, spectrum or directional-
12 ity of single emitters. The plasmonic approach has put most emphasis on the nanoscale antenna
13 element to control single emitter radiation^{1,2,22-24} *via* the strong electromagnetic enhancement in
14 the near field of metals. In contrast, the photonic crystal approach centers on the use of coher-
15 ent scattering to boost the interaction strength of intrinsically weakly scattering building blocks.
16 State-of-the-art structures use thin high index membranes perforated by nanoapertures, in which
17 the guided modes fold into a complex bandstructure. Spontaneous emission control then revolves
18 around the targeted coupling of an emitter to select Bloch modes, with well-controlled out-coupling
19 characteristics. Very recently, interest has emerged in the interplay between these two approaches,
20 implying the use of a coherent array of plasmonics resonators to shape the luminescence emission
21 properties. Two key examples are provided on one hand by the use of diffractive modes in 2D
22 arrays of plasmon particles to shape emission of thin emissive layers,^{10,11,25-27} and on the other
23 hand by the demonstration of Yagi-Uda antenna with a single quantum dot emitter in the optical
24 regime³, where coherent near field coupling between scattering nanoparticles is determinant to
25 achieve directional emission.⁶
26
27
28
29
30
31
32
33
34
35
36
37
38
39
40
41
42
43

44 Here, we investigate the emergence of coherent antenna array effects to shape the fluorescence
45 emission of single molecules in finite-sized bidimensional arrays of apertures milled into a metal
46 film that supports surface plasmon guided modes. Transmission properties of quasi-infinite aper-
47 ture arrays and single holes have been thoroughly investigated in the framework of extraordinary
48 optical transmission.²⁸ As reviewed by Garcia-Vidal and de Abajo,^{29,30} transmission measurements
49 show sharp, dispersive features that are frequently likened to a folding of the free surface plasmon
50 dispersion relation into a bandstructure, where the scattering potential that sets the interaction
51
52
53
54
55
56
57
58
59
60

1
2
3 strength is set by the single aperture polarizability. The influence of the array size was studied
4 by Przybilla³¹ and by Henzie.³² The transmission of just a small patch of nano-aperture lattice
5 is the well-known very broad single hole resonance, on which already for very small patches the
6 sharp features of extraordinary optical transmission are superimposed. As function of patch size,
7 these features sharpen and show small shifts. On basis of this work we examine if already in
8 small nano-aperture patches, periodic lattice physics controls phased array antenna design for sin-
9 gle molecules. We show the possibility of effective beamshaping by as few as 25 scatterers. In a
10 direct plasmonic analogy of photonic crystals milled in dielectrics, we consider hexagonal arrays
11 of nanoapertures milled in gold film, immersed in a dilute solution of fluorescent molecules (Fig-
12 ure 1). Only the central aperture is illuminated by a tightly focused pump laser beam. The driving
13 source for the fluorescence emission stands in the molecules located in the central aperture, which
14 serves as feed element for the rest of the antenna array. In this paper, we show that the plasmonic
15 crystal band structure of surface plasmon polaritons (SPP) is effective even in very small clusters
16 of apertures to tailor the radiation pattern of single molecules and provide a substantial absolute
17 increase in measured brightness per molecule. To support our experiment, we start from a general
18 model to calculate the radiation pattern for arbitrary arrangements of nano-apertures driven by a
19 single molecule, which enables the design of radiation patterns without symmetry constraints. For
20 the specific case of periodic arrangements as in our experiment, the calculation ultimately reduces
21 to a folding of the dispersion relation of the SPP dispersion into bands that emerges in the radi-
22 ation patterns. While formally, a band structure, *i.e.*, a sharp $\omega(k)$ relation, only exists in infinite,
23 lossless systems, in the plasmonic case, the band structure pertains to lossy modes (radiative loss
24 and absorptive loss). For perforated films, this band structure is well known, reveals itself in ex-
25 periments as broadened bands, and is close to the folded free surface plasmon dispersion relation,
26 in which narrow stop gaps open up.^{33–35} In agreement with our data and full wave simulations, the
27 model predicts strong directionality for frequencies near the closing of the second plasmon band,
28 at the center of the Brillouin zone. We find that the local density of photonic states (LDOS) en-
29 hancement that we measure, is independent of the lattice and primarily determined by the central
30
31
32
33
34
35
36
37
38
39
40
41
42
43
44
45
46
47
48
49
50
51
52
53
54
55
56
57
58
59
60

1
2
3 aperture. Fluorescence directionality and absolute extracted flux per molecule as caused by the
4 phased array behaviour, can thus be tuned independently from LDOS enhancement.
5
6

7 The significance of this study is twofold. First, from a conceptual point of view, it investigates
8 the build-up of directionality by coherent scattering in antenna arrays driven by a single emitter.
9
10 Second, from an application-driven point of view, we demonstrate enhanced directional emission
11 of fluorescence into a narrow angular cone that can be efficiently collected by a simple low nu-
12 merical aperture optical lens. On basis of fluorescence correlation spectroscopy data, we provide
13 quantitatively calibrated evidence of a large per-molecule brightness increase of 40 times in the
14 forward direction. This property is desirable to achieve high sensitivity fluorescence detection
15 with simple optical systems. The performance of our structures is on par with earlier work^{7,8,36}
16 that used nanoapertures surrounded by milled corrugations in so-called ‘bull’s eye’ configuration.
17 Conceptually, however, nanoaperture arrays have as major advantage that the emission character-
18 istics rigorously factorize in a single hole ‘structure factor’, and an ‘array factor’ that encodes the
19 geometric hole arrangement. This separation tremendously simplifies modeling, and opens up a
20 rich set of beam shaping design options for metasurface substrates, much alike to the beam shape
21 and polarization control possible with broad area photonic crystal emitters.²¹ Furthermore, we
22 note that the aperture arrays reported here are technically much simpler to fabricate, for instance
23 lending themselves to large-scale replication *via* soft conformal imprint techniques or template
24 stripping.^{37–39}
25
26
27
28
29
30
31
32
33
34
35
36
37
38
39
40
41
42
43
44

45 **Results and Discussion**

46
47 To obtain directed fluorescence emission normal to the sample plane, we design the plasmonic
48 band structure so that the center wavelength for fluorescence emission for our fluorophore (around
49 660 nm) falls near a plasmonic band edge that closes at the Γ -point ($k_{||} = 0$). This condition sets
50 the pitch between neighboring apertures to about one SPP wavelength. Specifically, we fabricated
51 optically thick gold films (150 nm thick) on a glass substrate, and drilled nanoapertures of 140
52
53
54
55
56
57
58
59
60

1
2
3 nm diameter in lattices of 440 nm pitch using focused ion beam milling. A series of samples
4 were generated with increasing number of rings of holes around a central aperture from 0 (single
5 aperture) to 3, placing the holes in a hexagonal lattice.
6
7
8

9
10 To record the influence of the plasmonic band structure on single molecule fluorescence emis-
11 sion, we cover each sample with a water solution containing Alexa Fluor 647 dyes at 1 μM concen-
12 tration (Figure 1a) which infiltrates the nano apertures. Diffusion ensures a continuous exchange
13 of fluorophores in the aperture with the reservoir in the droplet and thus avoids photobleaching of
14 the aperture fluorescence. The dipole orientation of the fluorophores in the liquid is random and
15 constantly changing. Thus all measured quantities are averages over the dipole orientation. The
16 sample is placed on a sample-scanning confocal inverted microscope, and excited using a laser
17 beam at 633 nm wavelength. As the confocal scan in Figure 1c shows, the different apertures
18 constituting the array are well resolved by our confocal setup. We obtain very bright fluorescence
19 with count rates above 300 kHz when exciting the center aperture, and counts below 1 kHz when
20 illuminating the gold film. Importantly, for each experiment reported below, we keep the position
21 of the sample fixed and centered on the laser focus, making sure to excite only the central hole of
22 each array. As part of our measurement protocol, prior to assessing directionality, we benchmark
23 the number of fluorescing molecules in the center aperture on basis of ‘fluorescence correlation
24 spectroscopy’.⁴⁰ This is performed by computing the second-order temporal correlation of the flu-
25 orescence intensity, as previously established.⁷ We find that for all structures, independently of the
26 total number of holes in the cluster, we detect almost the same number of contributing molecules
27 ($\langle N \rangle = 3.5 \pm 0.7$).
28
29
30
31
32
33
34
35
36
37
38
39
40
41
42
43
44
45

46 To analyze the angular fluorescence emission, we record the fluorescence intensity distribution
47 in the back focal plane (Fourier plane) of a 1.2 NA water immersion objective on a charge-coupled
48 device CCD camera. The radial coordinate in these images scales as the numerical aperture $\sin \theta$
49 for the emission, and thus the CCD images represent the intensity $I(\theta, \varphi)$ emitted from the plas-
50 monic crystal structure for different angular directions, where θ is measured from the sample nor-
51 mal and φ is the azimuthal angle. Figure 2 summarizes our main experimental results, namely, the
52
53
54
55
56
57
58
59
60

1
2
3 evolution of the radiation pattern as captured in the back focal plane images as a function of lattice
4 size. A single aperture (Fig. 2a,e) does not show any significant directional feature, although emis-
5 sion is more directional than a Lambertian emitter would be. In Fourier imaging with a high NA
6 aplanatic objective, a truly lambertian emitter would in fact show as a disk with highest intensity at
7 the edge of the BFP image.^{41,42} In stark contrast to the rather featureless single-hole radiation pat-
8 tern, when the central aperture is surrounded by three shells of holes, the radiation pattern appears
9 clearly structured (Figure 2d,h). In particular, a significant beaming is observed into the forward
10 direction, and the central beam is accompanied by a set of six side lobes reproducing the sixfold
11 symmetry of the lattice. Remarkably, we obtain directional emission despite the averaging over
12 the emitter orientations. On one hand this demonstrates robustness of the observed directionality,
13 while on the other hand further improvements might be possible if strategies to localize sources
14 on the nanoscale would be employed.³ Although only the center aperture is excited, the entire
15 lattice structure contributes to determine the angular distribution of the fluorescence emission. We
16 relate this strong directionality in the normal direction to constructive interferences between the
17 fluorescence light directly emitted from the central aperture into the far-field and the surface-wave
18 coupled fluorescence emission that is scattered into the far-field by the neighboring apertures. A
19 necessary condition for such constructive interference is that the aperture to aperture pitch corre-
20 sponds to approximately one SPP wavelength on the gold/glass interface. This condition can be
21 understood equivalently in k-space as requiring operation exactly at the condition of second or-
22 der Bragg diffraction for the surface plasmon wave, *i.e.*, at the closing of a plasmonic band near
23 the Γ -point of the lattice. Importantly, the observation of strong directionality demonstrates that
24 the neighboring apertures *coherently* re-emit the surface-wave fluorescence light stemming from a
25 single molecule. Incoherent superposition of the fluorescence light emitted by different molecules
26 would only result in the same featureless and broad radiation pattern observed for a single (iso-
27 lated) aperture.
28
29
30
31
32
33
34
35
36
37
38
39
40
41
42
43
44
45
46
47
48
49
50
51
52
53

54 To quantify the directionality relative to the sample normal, we average back focal plane images
55 over the azimuthal coordinate, taking into account the weighting caused by the objectives aplanatic
56
57
58
59
60

1
2
3 lens construction.⁴² Polar plots of the azimuthally averaged radiation patterns in Figure 2i demon-
4 strate increased directionality correlated with growing structure size, in excellent agreement with
5 the behavior expected for a coherent phased array antenna. On basis of the calibration of the av-
6 erage number of detected molecules for each sample, we can directly relate the radiation patterns
7 to detected photon flux *per molecule* and per solid angle.^{7,8} This quantifies the fluorescence en-
8 hancement along each emission direction. Furthermore, we can also compute the directivity figure
9 of merit for each antenna. In classical antenna theory, the directivity corresponds to the ratio of the
10 radiated power density along the direction of strongest emission relative to the power density radi-
11 ated by an ideal isotropic source emitting the same amount of total power.⁴³ For a single aperture,
12 we measure a fluorescence enhancement of 10x integrated over the whole collection numerical
13 aperture (as compared to the reference in solution without aperture), and a corresponding direc-
14 tivity of 3.4 dB.⁸ For a hexagonal lattice with three shells, we record a fluorescence enhancement
15 up to 40x into the forward direction, and a directivity of 4.3 dB. The enhancement and directivity
16 clearly increase with lattice size, as expected from a spatially distributed phased array effect.

17
18
19
20
21
22
23
24
25
26
27
28
29
30
31
32 That a hexagonal lattice provides strong directionality is expected since the radial distance
33 from the central aperture to the next row of apertures is uniquely defined, so that contributions
34 from all apertures sum up constructively. In other words, the hexagonal lattice benefits from an
35 almost circular Brillouin zone. This should be contrasted to the case of square lattices, that we also
36 investigated to further confirm the defining role of the band structure for the radiation pattern. We
37 performed measurement on square lattices of different sizes, all with the same pitch of $a = 440$ nm
38 as the hexagonal structures, and with the same hole size of 140 nm. Figure 3 shows scanning
39 electron micrographs of the fabricated square structures (total size 1, 5, 21, 37 unit cells). As
40 in the case of hexagonal arrays, we measured radiation patterns and observed increasing overall
41 collected flux per molecule as the structure size increases. However, the radiation pattern is best
42 characterized as a ring with a minimum into the forward direction. The maximum enhancement
43 of 2.8x for the square lattice is located at an angle of $\theta \approx 20^\circ$, whereas the enhancement into the
44 forward direction is only 1.9x. This stark contrast with the hexagonal lattice data can be interpreted
45
46
47
48
49
50
51
52
53
54
55
56
57
58
59
60

1
2
3 in k-space as firstly due to the Brillouin zone being more circular for the hexagonal case, and
4
5 secondly through the fact that at the same pitch, the square lattice reciprocal lattice vectors differ
6
7 by a factor of $\sqrt{3/4}$ in length.
8

9
10 We now return to the strongly directional radiation patterns evident for hexagonal lattices, and
11 compare our measurements to 3D electromagnetic simulations performed with the finite element
12 method using a commercial solver (see Methods section). Figure 4a presents the results for a
13 single aperture surrounded by two shells of apertures in a hexagonal lattice (corresponding to the
14 experiment depicted in fig. 2c,g). The simulated radiation patterns bear a substantial dependence
15 on the emission wavelength (we show in Figure 4b a fluorescence spectrum of Alexa Fluor 647
16 for reference). The radiation patterns show a marked transition from highly directional beaming
17 into the forward direction for wavelengths of 700 nm and above, to a redistribution of the radiated
18 power into six side lobes and no emission into the forward direction at wavelengths of 685 nm and
19 below. The experimental back focal plane images actually result from spectral averaging over the
20 range from 670 to 710 nm (grey shaded region in Fig. 4). This spectral averaging underlies our
21 experimental observation of strong beaming normal to the sample *accompanied by* six side lobes
22 for the hexagonal lattice.
23
24
25
26
27
28
29
30
31
32
33
34
35

36 To confirm experimentally the predicted spectral dependence of the radiation patterns, we
37 record the fluorescence spectrum after placing a diaphragm in the back focal plane to transmit
38 only the radiation of the inner lobe (corresponding to the green circle in Fig. 4a). We report spectra
39 for the structure analyzed in Fig. 2(d,h). The spectra with diaphragm (green solid line), without
40 diaphragm (magenta dashed line) and the reference solution (black solid line) show marked dif-
41 ferences in the region 700-740 nm. In particular, when we use the diaphragm to select only the
42 central lobe, the spectrum clearly shows an extra emission shoulder in the red, consistent with
43 the prediction from simulations that beaming is strong only for wavelengths to the red of a sharp
44 cut-off at 700 nm (Figure 4b). The differences are better clarified by computing the fluorescence
45 enhancement as compared to the confocal reference case (Fig. 4c). When only the central lobe is
46 selected, we observe a significant spectral enhancement for wavelengths above 700 nm, indicating
47
48
49
50
51
52
53
54
55
56
57
58
59
60

that the central lobe indeed contains significantly red-shifted fluorescence emission. This experimental finding stands in excellent agreement with the predictions from the simulated radiation patterns.

On basis of measurements and simulations, we conclude that the hexagonal clusters of apertures realize a nanoscale phased array antenna, where the required coupling between scatterers must be mediated *via* surface plasmon polaritons. To underpin this claim with a simple analytical model, we use a classical result from radiowave antenna theory.^{42,43} In the far-field of a phased array antenna of identical elements, the electric field along an observation direction \hat{k} (vector of unit length) can be written as

$$\mathbf{E} = \frac{e^{ikR}}{R} S(\hat{k}) \sum_{n=1}^N A_n e^{-i\mathbf{k}\cdot\mathbf{r}_n} \quad (1)$$

where R is the radius of the observation sphere, and $\mathbf{k} = \omega/c\hat{k}$. Here, the first term is an overall spherical wave, and the second term $S(\hat{k})$ is the form factor of each single element, which is in the case of a single nano aperture almost but not perfectly isotropic,³⁶ and corresponds to the measured radiation pattern in Fig. 2e. The final term is the structure factor that is determined by the positions \mathbf{r}_n and complex amplitudes A_n of the scatterers. If we set the apertures to be driven through the surface plasmon (SPP) waves launched at the central aperture, we can assume a complex amplitude $A_n = \frac{Ae^{ik_{SPP}r_n}}{\sqrt{r_n}}$. Importantly, the finite structure phased array response is intimately related to the infinite-lattice band structure. If we lump the finite lattice truncation and the $1/\sqrt{r}$ decay together in a windowing function W_N we can rewrite Eq. (1) as

$$\mathbf{E} = \left[\frac{e^{ikR}}{R} S(\hat{k}) \right] \left[W_N \star \sum_{\text{lattice}} e^{i(k_{SPP}r_n - \mathbf{k}\cdot\mathbf{r}_n)} \right] \quad (2)$$

As recognized by Rigneault⁴⁴ the infinite sum over the entire lattice \mathbf{k} is formally equivalent to Harrison's construction⁴⁵ for the repeated zone scheme dispersion of the surface plasmon dispersion relation. For an infinite, lossless lattice, the infinite sum results in a discrete set of circles of radius k_{SPP} centered at the reciprocal lattice vectors. The rigorous band structure beyond the

1
2
3
4
5
6
7
8
9
10
11
12
13
14
15
16
17
18
19
20
21
22
23
24
25
26
27
28
29
30
31
32
33
34
35
36
37
38
39
40
41
42
43
44
45
46
47
48
49
50
51
52
53
54
55
56
57
58
59
60

folded free surface plasmon dispersion approximation was defined and calculated by Lalanne *et al.*³⁵ For the finite, lossy lattices studied here, the truncation windowing translates into a blurring of the infinite lattice band structure, formalized as a convolution with the Fourier transform \mathcal{W}_N of the truncation W_N .

Figure 5 shows the folded dispersion relation as a ω, k -diagram, where we calculate k_{SPP} from the surface plasmon dispersion on the Au/glass interface. As per the design choice of lattice pitch, we expect the dispersion relation to cross the Γ -point in the dye emission spectrum, at 650 nm within the free SPP approximation. In a system with finite interaction strength one expects a red shift of the entire dispersion relation,³⁵ and the opening of a small stop gap at the edge of the Brillouin-zone, that pushes the lower band edge further to the red.^{11,29,33,46} For frequencies below the band edge, the allowed modes lie on a ring of wave vector close to $k_{\parallel} = 0$. As the wavelength sweeps from 750 nm to ~ 700 nm, we hence expect increasing directionality as the ring closes. As the band edge is crossed, emission is funneled into the next higher order band that doesn't close at the Γ -point. Consequently, a steep transition in the radiation pattern is expected to occur from a single lobe, to a six-lobed radiation pattern, as is indeed predicted by the full-wave simulations. We refer to the Supplementary Information for a complete theoretical analysis for the square lattice case (data reported in Figure 3). In brief, for square lattices the Γ – point crossing of the square lattice is redshifted out of the dye emission spectrum. Instead the fluorescence is coincident with the next higher band, hence exiting the sample off normal. Full wave simulations further confirm the observed radiation patterns, and reveal that square lattices allow directional emission normal to the sample further to the IR, commensurate with the redshifted band edge.

Finally, for completeness, we also have measured the local density of states enhancement that the nano-aperture arrays provide. From the field of photonic crystals it is well known that redirection effects are not necessarily related to strong LDOS modifications. For instance, already at moderate index contrast marked redirection of emission, diffraction, and band-edge slow down of light^{47–50} can occur although variations in spontaneous emission rates in such systems are small.^{51,52} For both the hexagonal and square samples, and for all patch sizes, we have measured

1
2
3 fluorescence decay traces using time correlated single photon counting, pumping with a 636 nm
4 pulsed diode laser. Independent of array type or size, we record fluorescence lifetimes in the range
5 $\tau = 0.49 \pm 0.01$ ns (Fig. 6). Comparison with the lifetime of the open solution of $\tau_{\text{open}} = 1.03$ ns
6 yields a significant shortening of the lifetime in the nano-aperture by a factor of 2.1. Through
7 the known internal quantum efficiency, the measured *total* decay rate can be separated as the sum
8 of an intrinsic nonradiative decay rate that is not modified by photonic environment, and the in-
9 trinsic radiative rate on which the photonic environment acts,²² where by definition the change
10 exactly equals the LDOS normalized to the vacuum LDOS. Here the LDOS is rigorously defined
11 as the imaginary part of the Greens function $\Im(G(\mathbf{r}_0, \mathbf{r}_0))$ and contains the sum of all decay chan-
12 nels provided by the photonic environment,⁴¹ including those related to decay into any plasmonic
13 modes with strong near field enhancement, decay directly into the radiative continuum, and any
14 quenching that is induced by the vicinity of the metal. Since the quantum efficiency of Alexa
15 Fluor 647 is $\eta = 33\%$, we conclude that in all experiments, the molecules experience a significant
16 LDOS enhancement by a factor $\frac{1}{\eta}(\frac{\tau_{\text{open}}}{\tau} - 1 + \eta) = 4.4$. Importantly, we find that the measured
17 LDOS inside the central aperture is virtually independent of the lattice structure and not altered by
18 the formation of a SPP band structure. Since Wenger *et al.*⁵³ already reported a complete study
19 of the radiative and non-radiative decay channels in single nanoapertures, we don't pursue a de-
20 composition into the distinct contributions that add up to the measured LDOS change here. The
21 important conclusion for this work is that the nanophotonic control factorizes into two effects. On
22 one hand directionality control and an increase in absolute count rate per molecule is provided *via*
23 coherent reradiation by the entire phased array. As in the case of moderate index photonic crystals,
24 this redirection effect is strong, although the periodicity has no strong effect on LDOS. Indeed, the
25 LDOS is governed entirely by the geometry of the hole to which the fluorophore is directly cou-
26 pled. A similar factorization to facilitate nanophotonic design was noted for plasmonic Yagi-Uda
27 antennas, where the entire array determines the overall directivity, while Purcell enhancement can
28 be independently engineered by modifying only the feed element.⁶
29
30
31
32
33
34
35
36
37
38
39
40
41
42
43
44
45
46
47
48
49
50
51
52
53
54
55
56
57
58
59
60

Conclusions

Hexagonal clusters of nano-apertures in a plasmonic film realize a nanoscale phased array antenna to control single molecule emission. The formation of a plasmonic band structure is a simple and powerful tool to tailor the radiation patterns of localized single emitters, enabling up to 40 times brightness enhancement per molecule in the forward direction in our experiment. We demonstrate that already small lattices with less than 25 elements show such highly directional emission that is set by the plasmonic crystal band structure, in excellent correspondence with numerical simulations. Interestingly, the single emitter radiation pattern can be tuned independently from the LDOS, as the 4.4-fold Purcell enhancement factor depends only on the geometry of the central hole that acts as feed element for the entire antenna.

Strong directionality of emission was reported earlier in two distinct plasmonic scenarios: on one hand for Yagi-Uda antennas that are interpreted as a travelling wave phased array antenna, and on the other hand for emission of ensembles of fluorophores tuned to diffraction resonances in infinite periodic arrays.^{10,11,25–27} Here, we show that the very same mechanisms that are explored for infinite arrays of scatterers are already at play in small phased array antennas, as the band structure is evident in the emission pattern of single emitters in very small clusters of scatterers that are just a few unit cells across. This demonstration that infinite-system dispersion relations of diffractive modes can be used to tailor the behavior of phased array antennas that are very limited in size is complementary to the finding for Yagi-Uda antennas that directionality results from the infinite 1D chain dispersion relation.^{3,6} While Yagi-Uda antennas are limited to on-axis beaming, diffractive arrays allow much larger flexibility for beam steering, beam shaping and polarization control. Thereby our work opens a rich toolbox to engineer single photon emitters to emit selectively in particular angles, polarization states, or in more exotic beam profiles such as doughnut modes or orbital angular momentum beams. As compared to surface groove milling,^{7,8,36} the fabrication of array of apertures appears as a much simpler and robust technical solution. Indeed, while the structures presented in this manuscript were prototyped with focused ion beam milling, they can be manufactured on large scale using replication techniques such as imprint lithography.^{37–39}

Methods

Nanofabrication

Our samples consist of a metal film deposited on a glass cover slide (Menzel Gläser #1.5, thickness: 0.17 ± 0.01 mm) by thermal evaporation. We first evaporated 2 nm chromium and then 150 nm gold (10^{-6} mbar, 0.6 \AA/s). Several arrays of nano-apertures (140 nm) were milled into the metal film by focused ion beam (FIB) milling. In particular, the arrays are small periodic lattices of hexagonal (1, 7, 19, 37 unit cells; Fig. 2(a-d)) of 440 nm pitch.

Experimental setup

The experimental setup is based on a confocal inverted microscope with a NA= 1.2 water-immersion objective. The sample is mounted on a computer controlled XYZ piezo stage (Polytech PI P-517.3CD) and dye-solution ($\approx 1 \mu\text{molar}$ Alexa647 in standard phosphate-buffered saline (PBS) solution) is dropped on the sample and infiltrates the nano-apertures. A He-Ne laser ($\lambda_{\text{HeNe}} = 633\text{nm}$, continuous wave (CW)) is focused with a water immersion objective (Zeiss C-apochromat 40x, NA = 1.2) on the sample through the glass slide. For lifetime measurements, the excitation source is a picosecond laser diode operating at 636 nm (PicoQuant LDH-P-635, repetition rate 80 MHz). A single-mode optical fiber (Thorlabs P3-630A-FC-5) ensures a perfect spatial overlap between the pulsed laser diode and the CW He-Ne laser. The fluorescence signal is collected through the same objective and is separated from the pump laser light at a dichroic mirror. For confocal imaging and FCS we employ a $30 \mu\text{m}$ pinhole (effectively 375 nm in the sample plane). Single photon detection is performed by avalanche photodiodes (Micro Photon Devices MPD-5CTC) in a Hanbury-Brown Twiss (HBT) configuration featuring a band pass filter (Omega Filters 640AELP) in front of each APD to further remove all scattered laser light. The fluorescence intensity temporal fluctuations are analyzed with a ALV6000 hardware correlator which computes the second order correlation function. We determine the average number of molecules contributing to the signal by fitting the analytical expression⁵³ for free diffusion FCS.

1
2
3
4 For radiation pattern imaging a mirror just after the dichroic mirror directs the fluorescence
5 emission through a band pass filter (690 ± 20 nm) on a camera (Kodak KAF-1603, CCD with
6 microlenses). The optical path between objective and CCD contains only bandpass filtering ($690 \pm$
7 20 nm), but no lenses, and is about 1 m in length. In the backfocal plane (BFP) the intensity
8 distribution corresponds to the angular emission pattern or 'fourier image' of the structure in the
9 focal plane.⁵⁴ We reconstruct a polar plot of radiated flux per solid angle by averaging the radiated
10 power over the azimuthal angle φ and compensating for the $1/\cos\theta$ response associated with
11 backaperture imaging of aplanatic lens systems.^{41,42}

12
13
14
15
16
17
18
19
20 For fluorescence lifetime measurements, the APD output is coupled to a fast time-correlated
21 single photon counting module (PicoQuant PicoHarp 300) and correlated against the electronic
22 trigger output of the pulsed laser diode. The temporal resolution of our setup for fluorescence
23 lifetime measurements is 120 ps FWHM. Finally, for measuring the antenna's influence on the
24 fluorescence spectrum, fluorescence was sent to a spectrograph (Horiba iHR320) equipped with
25 a Peltier-cooled CCD detector. To measure the spectrum of the inner lobe of the fluorescence
26 emission, a diaphragm ($\varnothing 2.9$ mm) was inserted into the beampath right after the dichroic and
27 aligned with the CCD. The diameter of the collimated beam of the entire BFP is ≈ 9 mm. The
28 raw spectrum is normalized by the number of molecules given by correlation analysis, which
29 allows to directly compare the fluorescence enhancement as a function of emission wavelength.
30 The Supporting Information contains a full set up diagram, and a description of the measurement
31 protocol.
32
33
34
35
36
37
38
39
40
41
42
43
44
45

46 Numerical simulations

47
48
49 Full wave calculations of radiation pattern were obtained using the COMSOL 4.3 finite element
50 solver. As refractive indices we assume $n = 1.33$, $n = 1.52$ for water and glass, and a modified
51 Drude model $\epsilon = \epsilon_b - \frac{\omega_p^2}{(\omega^2 + i\omega\gamma)}$ for gold,⁵⁵ with $\epsilon_b = 9.54$, $\omega_p = 2\pi \cdot 2.148 \cdot 10^{15}$ Hz and $\gamma =$
52 $0.0092 \cdot \omega_p$. As simulation domain we use a cylinder with axis normal to the sample substrate
53 that is a stack of water and the perforated gold film, on top of which we place a hemispherical
54
55
56
57
58
59
60

1
2
3 dome of glass (representative real space geometry shown in the Supporting Information). The
4 simulation domain is closed on all sides with perfectly matched layers ($\sim \lambda/2$ thickness), and has
5 a radius of $2 \mu\text{m}$ (approximately 4 wavelengths). As source we place a current-carrying dipole
6 in the center of the central hole mimicking the fluorescent molecule. For dipoles located on the
7 central axis, we can employ symmetry to reduce the computation load, having to solve only in
8 the $x > 0, y > 0$ quadrant and employing perfect electric/magnetic boundary conditions on the
9 symmetry planes as appropriate. We retrieve the far field by performing a Stratton-Chu near to far
10 field transformation⁵⁶ of the fields that we calculate on the glass side on a spherical cap concentric
11 with the central hole, that has a radius of $1.33 \mu\text{m}$ (3 wavelengths as measured in glass) and is
12 truncated 300 nm above the sample surface. It should be noted that in presence of a substrate,
13 the Stratton-Chu near to far field transformation is not rigorous, and the results are hence a finite-
14 truncation radius approximation to the angular spectrum representation integral that rigorously
15 describes radiation patterns near surfaces. On basis of benchmark comparisons of this approach to
16 theory for dipole sources above unpatterned interfaces,^{57,58} we estimate accuracy to within 10 –
17 20 %. We obtain ensemble averaging over random dipole orientation rigorously by summing the
18 calculated angle-resolved far field fluxes over three orthogonal dipole orientations for which we
19 do the simulations. In practice we found that the z-oriented dipole hardly contributes to far field
20 radiation in both the hexagonal and square lattice, pointing to a large difference in radiative LDOS.
21
22
23
24
25
26
27
28
29
30
31
32
33
34
35
36
37
38
39
40
41

42 **Conflict of Interest:**

43
44
45 The authors declare no competing financial interest.
46
47

48 **Acknowledgement**

49
50
51 We are grateful to Martin Frimmer, Clara Osorio, Nicolas Bonod and Hervé Rigneault for stim-
52 ulating discussions. We acknowledge a “Van Gogh” grant of the “Frans-Nederlandse Academie
53 (FNA)” and the “Réseau Franco-Néerlandais (RFN)” for facilitating exchange visits. This work
54 is part of the research program of the “Foundation for Fundamental Research on Matter (FOM)”,
55
56
57
58
59
60

1
2
3 which is financially supported by the “The Netherlands Organization for Scientific Research (NWO)”.
4
5 This work is supported by NanoNextNL, a micro and nanotechnology consortium of the Govern-
6
7 ment of the Netherlands and 130 partners. AFK gratefully acknowledges an NWO-Vidi grant for
8
9 financial support. The research leading to these results has received funding from the European
10
11 Commission’s Seventh Framework Programme (FP7-ICT-2011-7) under grant agreements 288263
12
13 (NanoVista) and ERC StG 278242 (ExtendFRET).
14
15
16

17 18 **Supporting Information Available**

19
20 Measurement protocol, calibration FCS measurements, radiation patterns and SEM images mea-
21
22 sured on square arrays, and further detail on the COMSOL simulation procedure. This material is
23
24 available free of charge *via* the Internet at <http://pubs.acs.org>.
25
26
27

28 29 **References**

- 30
31 1. Agio, M.; Alú, A., Eds. *Optical Antennas*; Cambridge University Press, 2013.
- 32
33
34 2. Kinkhabwala, A.; Yu, Z.; Fan, S.; Avlasevich, Y.; Müllen, K.; Moerner, W. E. Large Single-
35
36 Molecule Fluorescence Enhancements Produced by a Bowtie Nanoantenna. *Nat. Photonics*
37
38 **2009**, *3*, 654–657.
- 39
40
41 3. Curto, A. G.; Volpe, G.; Taminiau, T. H.; Kreuzer, M. P.; Quidant, R.; van Hulst, N. F. Unidi-
42
43 rectional Emission of a Quantum Dot Coupled to a Nanoantenna. *Science* **2010**, *329*, 930–933.
- 44
45
46 4. Kosako, T.; Kadoya, Y.; Hofmann, H. F. Directional Control of Light by a Nano-optical Yagi-
47
48 Uda Antenna. *Nat. Photonics* **2010**, *4*, 312–315.
- 49
50
51 5. Taminiau, T. H.; Stefani, F. D.; Segerink, F. B.; van Hulst, N. F. Optical Antennas Direct
52
53 Single-Molecule Emission. *Nat. Photonics* **2008**, *2*, 234–237.
- 54
55
56 6. Koenderink, A. F. Plasmon Nanoparticle Array Waveguides for Single Photon and Single Plas-
57
58 mon Sources. *Nano Lett.* **2009**, *9*, 4228–4233.
- 59
60

- 1
2
3
4
5
6
7
8
9
10
11
12
13
14
15
16
17
18
19
20
21
22
23
24
25
26
27
28
29
30
31
32
33
34
35
36
37
38
39
40
41
42
43
44
45
46
47
48
49
50
51
52
53
54
55
56
57
58
59
60
7. Aouani, H.; Mahboub, O.; Bonod, N.; Devaux, E.; Popov, E.; Rigneault, H.; Ebbesen, T. W.; Wenger, J. Bright Unidirectional Fluorescence Emission of Molecules in a Nanoaperture with Plasmonic Corrugations. *Nano Lett.* **2011**, *11*, 637–644.
8. Aouani, H.; Mahboub, O.; Devaux, E.; Rigneault, H.; Ebbesen, T. W.; Wenger, J. Plasmonic Antennas for Directional Sorting of Fluorescence Emission. *Nano Lett.* **2011**, *11*, 2400–2406.
9. Belacel, C.; Habert, B.; Bigourdan, F.; Marquier, F.; Hugonin, J.-P.; Michaelis de Vasconcellos, S.; Lafosse, X.; Coolen, L.; Schwob, C.; Javaux, C. *et al.* Controlling Spontaneous Emission with Plasmonic Optical Patch Antennas. *Nano Lett.* **2013**, *13*, 1516–1521.
10. Vecchi, G.; Giannini, V.; Gómez Rivas, J. Shaping the Fluorescent Emission by Lattice Resonances in Plasmonic Crystals of Nanoantennas. *Phys. Rev. Lett.* **2009**, *102*, 2–5.
11. Lozano, G.; Louwers, D. J.; Rodriguez, S.; Murai, S.; Jansen, O. T. A.; Verschuuren, M.; Rivas, J. G. Plasmonics for Solid-State Lighting: Enhanced Excitation and Directional Emission of Highly Efficient Light Sources. *Light: Sci. Appl.* **2013**, *2*, e66.
12. Busch, K.; John, S. Photonic Bandgap Formation in Certain Selforganizing Systems. *Phys. Rev. E* **1998**, *58*, 3896–3908.
13. Koenderink, A. F.; Bechger, L.; Schriemer, H. P.; Lagendijk, A.; Vos, W. L. Broadband Fivefold Reduction of Vacuum Fluctuations Probed by Dyes in Photonic Crystals. *Phys. Rev. Lett.* **2002**, *88*, 143903.
14. Fujita, M.; Takahashi, S.; Tanaka, Y.; Takashi, A.; Noda, S. Simultaneous Inhibition and Redistribution of Spontaneous Light Emission in Photonic Crystals. *Science* **2005**, *308*, 1296–1298.
15. Lodahl, P.; van Driel, A. F.; Nikolaev, I. S.; Irman, A.; Overgaag, K.; Vanmaekelbergh, D.; Vos, W. L. Controlling the Dynamics of Spontaneous Emission from Quantum Dots by Photonic Crystals. *Nature* **2004**, *430*, 654–657.

16. Wang, Q.; Stobbe, S.; Lodahl, P. Mapping the Local Density of Optical States of a Photonic Crystal with Single Quantum Dots. *Phys. Rev. Lett.* **2011**, *107*, 167404.
17. Jorgensen, M. R.; Galusha, J. W.; Bartl, M. H. Strongly Modified Spontaneous Emission Rates in Diamond-Structured Photonic Crystals. *Phys. Rev. Lett.* **2011**, *107*, 143902.
18. Noda, S.; Fujita, M.; Asano, T. Spontaneous-Emission Control by Photonic Crystals and Nanocavities. *Nat. Photonics* **2007**, *1*, 449–458.
19. Barth, M.; Nüsse, N.; Löchel, B.; Benson, O. Controlled Coupling of a Single-Diamond Nanocrystal to a Photonic Crystal Cavity. *Opt. Lett.* **2009**, *34*, 1108–1110.
20. Aoki, K.; Guimard, D.; Nishioka, M.; Nomura, M.; Iwamoto, S.; Arakawa, Y. Coupling of Quantum-Dot Light Emission with a Three-Dimensional Photonic-crystal Nanocavity. *Nat. Photonics* **2008**, *2*, 688–692.
21. Noda, S. Photonic Crystal Lasers - Ultimate Nanolasers and Broad-Area Coherent Lasers [Invited]. *J. Opt. Soc. Am. B* **2010**, *27*, B1–B8.
22. Mertens, H.; Koenderink, A. F.; Polman, A. Plasmon-Enhanced Luminescence Near Noble-Metal Nanospheres: Comparison Of Exact Theory and an Improved Gersten and Nitzan Model. *Phys. Rev. B* **2007**, *76*, 115123.
23. Ming, T.; Zhao, L.; Chen, H.; Woo, K. C.; Wang, J.; Lin, H.-Q. Experimental Evidence of Plasmaphores: Plasmon-Directed Polarized Emission From Gold Nanorod-Fluorophore Hybrid Nanostructures. *Nano Lett.* **2011**, *11*, 2296–2303.
24. Ming, T.; Chen, H.; Jiang, R.; Li, Q.; Wang, J. Plasmon-Controlled Fluorescence: Beyond the Intensity Enhancement. *J. Phys. Chem. Lett.* **2012**, *3*, 191–202.
25. Wedge, S.; Hooper, I. R.; Sage, I.; Barnes, W. L. Light Emission through a Corrugated Metal Film: The Role of Cross-Coupled Surface Plasmon Polaritons. *Phys. Rev. B* **2004**, *69*, 245418.

- 1
2
3
4 26. Rodriguez, S.; Murai, S.; Verschuuren, M.; Gómez Rivas, J. Light-Emitting Waveguide-
5 Plasmon Polaritons. *Phys. Rev. Lett.* **2012**, *109*, 166803 1–5.
6
7
8
9 27. Zayats, A. V.; Smolnyaninov, I. I.; Maradudin, A. A. Nano-Optics of Surface Plasmon Polari-
10 tons. *Phys. Rep.* **2005**, *408*, 131–314.
11
12
13 28. Ebbesen, T. W.; Lezec, H. J.; Ghaemi, H. F.; Thio, T.; Wolff, P. A. Extraordinary Optical
14 Transmission Through Sub-Wavelength Hole Arrays. *Nature* **1998**, *391*, 667–669.
15
16
17
18 29. García de Abajo, F. J. Colloquium: Light Scattering by Particle and Hole Arrays. *Rev. Mod.*
19 *Phys.* **2007**, *79*, 1267–1290.
20
21
22
23 30. Garcia-Vidal, F. J.; Ebbesen, T. W.; Kuipers, L. Light Passing Through Subwavelength Aper-
24 tures. *Rev. Mod. Phys.* **2010**, *82*, 729–787.
25
26
27
28 31. Przybilla, F.; Degiron, a.; Genet, C.; Ebbesen, T.; de León-Pérez, F.; Bravo-Abad, J.; García-
29 Vidal, F. J.; Martín-Moreno, L. Efficiency and Finite Size Effects in Enhanced Transmission
30 through Subwavelength Apertures. *Opt. Expr.* **2008**, *16*, 9571–9579.
31
32
33
34 32. Henzie, J.; Lee, M. H.; Odom, T. W. Multiscale Patterning of Plasmonic Metamaterials. *Nature*
35 *Nanotechnol.* **2007**, *2*, 549–554.
36
37
38
39 33. Kitson, S.; Barnes, W.; Sambles, J. Full Photonic Band Gap for Surface Modes in the Visible.
40 *Phys. Rev. Lett.* **1996**, *77*, 2670–2673.
41
42
43
44 34. Barnes, W. L.; Kitson, S. C.; Preist, T. W.; Sambles, J. R. Photonic Surfaces for Surface-
45 Plasmon Polaritons. *J. Opt. Soc. Am. A* **1997**, *14*, 1654.
46
47
48
49 35. Lalanne, P.; Rodier, J. C.; Hugonin, J.-P. Surface Plasmons of Metallic Surfaces Perforated by
50 Nanoholes. *J. Opt. A - Pure Appl. Opt.* **2005**, *7*, 422–426.
51
52
53
54 36. Jun, Y. C.; Huang, K. C. Y.; Brongersma, M. L. Plasmonic Beaming and Active Control Over
55 Fluorescent Emission. *Nat. Commun.* **2011**, *2*, 283.
56
57
58
59
60

- 1
2
3
4
5
6
7
8
9
10
11
12
13
14
15
16
17
18
19
20
21
22
23
24
25
26
27
28
29
30
31
32
33
34
35
36
37
38
39
40
41
42
43
44
45
46
47
48
49
50
51
52
53
54
55
56
57
58
59
60
37. Verschuuren, M.; Gerlach, P.; van Sprang, H. A.; Polman, A. Improved Performance of Polarization-Stable VCSELs by Monolithic Sub-Wavelength Gratings Produced by Soft Nano-Imprint Lithography. *Nanotechn.* **2011**, *22*, 505201.
 38. Nagpal, P.; Lindquist, N. C.; Oh, S. H.; Norris, D. J. Ultrasmooth Patterned Metals for Plasmonics and Metamaterials. *Science* **2009**, *325*, 594–597.
 39. Henzie, J.; Lee, J.; Lee, M. H.; Hasan, W.; Odom, T. W. Nanofabrication of Plasmonic Structures. *Annu. Rev. Chem.* **2009**, *60*, 147–165.
 40. Schwille, P.; Bieschke, J.; Oehlschläger, F. Kinetic Investigations by Fluorescence Correlation Spectroscopy: the Analytical and Diagnostic Potential of Diffusion Studies. *Biophys. Chem.* **1997**, *66*, 211–228.
 41. Novotny, L.; Hecht, B. *Principles of Nano Optics*; Cambridge University Press, 2006.
 42. Sersic, I.; Tuambilangana, C.; Koenderink, A. F. Fourier Microscopy of Single Plasmonic Scatterers. *New J. Phys.* **2011**, *13*, 083019.
 43. Balanis, C. A. *Antenna Theory: Analysis and Design (3rd edition)*; John Wiley & Sons, Hoboken, New Jersey, 2005.
 44. Rigneault, H.; Lemarchand, F.; Sentenac, A.; Giovannini, H. Extraction of Light from Sources Located Inside Waveguide Grating Structures. *Opt. Lett.* **1999**, *24*, 148–150.
 45. Harrison, W. A. *Solid State Theory*; Dover Publications, 1970.
 46. Kretschmann, M.; Maradudin, a. Band Structures of Two-Dimensional Surface-Plasmon Polaritonic Crystals. *Phys. Rev. B* **2002**, *66*, 245408.
 47. Nikolaev, I.; Lodahl, P.; Vos, W. Quantitative Analysis of Directional Spontaneous Emission Spectra from Light Sources in Photonic Crystals. *Phys. Rev. A* **2005**, *71*, 053813.

- 1
2
3
4 48. Barth, M.; Gruber, A.; Cichos, F. Spectral and Angular Redistribution of Photoluminescence
5 Near a Photonic Stop Band. *Phys. Rev. B* **2005**, *72*, 085129.
6
7
8
9 49. Garcia-Santamaria, F.; Galisteo-López, J. F.; Braun, P. V.; López, C. Optical Diffraction
10 and High-Energy Features in Three-Dimensional Photonic Crystals. *Phys. Rev. B* **2005**, *71*,
11 195112.
12
13
14
15 50. Galisteo-López, J. F.; Galli, M.; Patrini, M.; Balestreri, A.; Andreani, L. C.; López, C. Effec-
16 tive Refractive Index and Group Velocity Determination of 3D Photonic Crystals by Means of
17 White Light Interferometry. *Phys. Rev. B* **2006**, *73*, 125103.
18
19
20
21
22 51. Li, Z.-Y.; Zhang, Z.-Q. Weak Photonic Band Gap Effect on the Fluorescence Lifetime in
23 Three-Dimensional Colloidal Photonic Crystals. *Phys. Rev. B* **2001**, *63*, 125106.
24
25
26
27 52. Nikolaev, I.; Lodahl, P.; Vos, W. Fluorescence Lifetime of Emitters with Broad Homogeneous
28 Linewidths Modified in Opal Photonic Crystals. *J. Phys. Chem. C* **2008**, *112*, 7250–7254.
29
30
31
32 53. Wenger, J.; Gérard, D.; Dintinger, O., J. and Mahboub; Bonod, N.; Popov, E.; Ebbesen, T. W.;
33 Rigneault, H. Emission and Excitation Contributions to Enhanced Single Molecule Fluores-
34 cence by Gold Nanometric Apertures. *Opt. Expr.* **2008**, *16*, 3008.
35
36
37
38
39 54. Saleh, B. E. A.; Teich, M. C. *Fundamentals of Photonics - 2nd ed.*; Wiley and Sons, Hoboken,
40 New Jersey, 2007; Chapter 4.
41
42
43
44 55. Penninkhof, J. J.; Moroz, A.; van Blaaderen, A.; Polman, A. Optical Properties of Spherical
45 and Oblate Spheroidal Gold Shell Colloids. *J. Phys. Chem. C* **2008**, *112*, 4146–4150.
46
47
48
49 56. Taflove, A.; Hagness, S. C. *Computational Electrodynamics: The Finite-Difference Time-*
50 *Domain Method*, 3rd ed.; Artech House Publishers, 2005; Chapter 8.
51
52
53
54 57. Lukosz, W.; Kunz, R. E. Light Emission by Magnetic and Electric Dipoles Close to a Plane
55 Interface. I. Total Radiated Power. *J. Opt. Soc. Am.* **1977**, *67*, 1607–1615.
56
57
58
59
60

- 1
2
3
4 58. Lukosz, W.; Kunz, R. E. Light Emission by Magnetic and Electric Dipoles Close To A Plane
5 Dielectric Interface. II. Radiation Patterns of Perpendicular Oriented Dipoles. *J. Opt. Soc. Am.*
6 **1977**, *67*, 1615–1619.
7
8
9
10
11
12
13
14
15
16
17
18
19
20
21
22
23
24
25
26
27
28
29
30
31
32
33
34
35
36
37
38
39
40
41
42
43
44
45
46
47
48
49
50
51
52
53
54
55
56
57
58
59
60

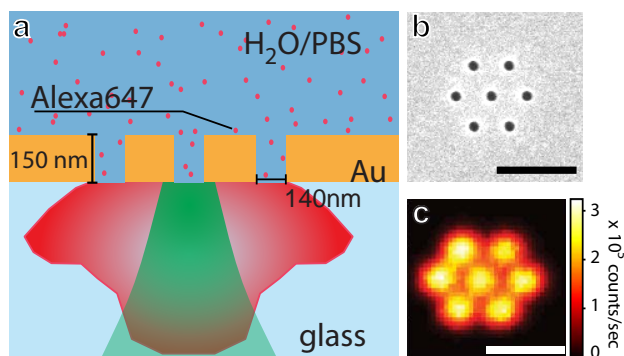


Figure 1: (a) Sketch of the sample consisting of a 150 nm thick gold film on glass with apertures of 140 nm diameter at 440 nm pitch. A drop of 1 μ M solution of Alexa Fluor 647 in water saline solution is placed on top of the sample. (b) SEM image and (c) confocal fluorescence scan of a hexagonal array consisting of a central hole with one shell of apertures around it. The scale bars correspond to 1 μ m.

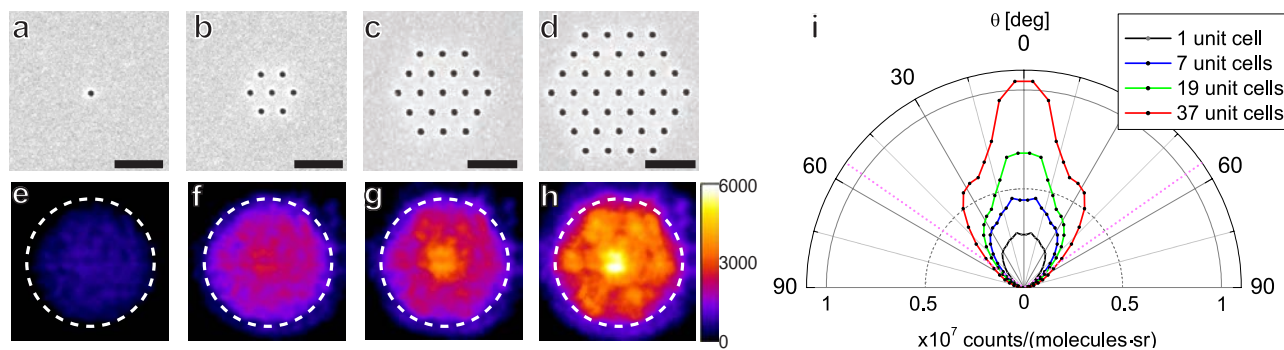


Figure 2: (a) Scanning electron micrographs of a single hole structure, and hexagonal clusters with (b) 7, (c) 19 and (d) 37 unit cells (one, two and three shells) around the central aperture (the scale bar is $1\mu\text{m}$). (e-h) Back focal plane (Fourier plane) images representing the radiation patterns for the structures in (a-d). Note that only the central aperture was illuminated by the laser beam in these experiments. The colorbar represents a linear scale from 0 to 6000 counts per pixel. (i) Radiated intensity in counts per second per molecule per solid angle for hexagonal lattices of increasing number of apertures.

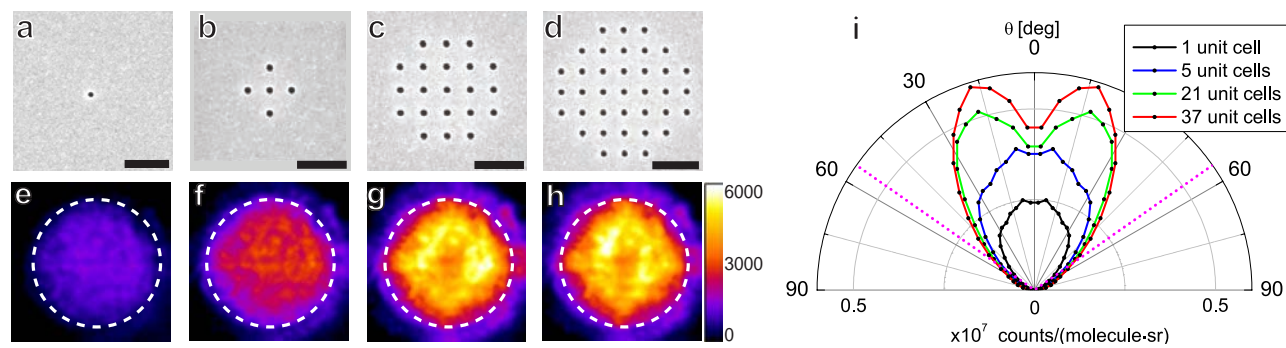


Figure 3: (a-e) Scanning electron micrographs of square lattices of different size (scalebar: $1\mu\text{m}$), (e-h) corresponding radiation patterns and i) radiated intensity per molecule per steradian.

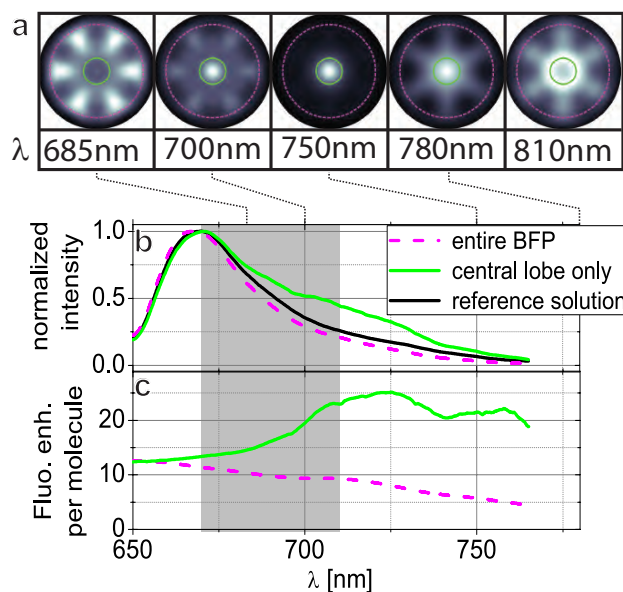


Figure 4: (a) Computed radiation patterns into the glass substrate for selected wavelengths assuming an isotropic ensemble of emitting dipoles in the central aperture surrounded by two shells of apertures in hexagonal lattice. (b) Normalized fluorescence spectra after placing a diaphragm (corresponding to the green circle in panel a) in the back focal plane to transmit only the radiation of the inner lobe. The reference solution spectrum appears in black, the hexagonal cluster with two shells and open diaphragm (full angular integration) is shown in magenta dashed line, and the closed diaphragm case is displayed in solid green line. (c) Enhancement of the fluorescence intensity per molecule with an open (magenta dashed line) or closed diaphragm (solid green line).

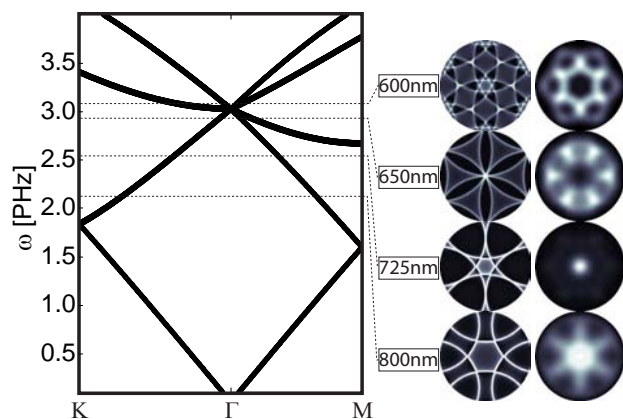


Figure 5: Band diagram of the folded dispersion relation of a hexagonal 2D lattice with zero interaction. Note that the vertical axis is in normalized frequency units d/λ_{SPP} , where in fact λ_{SPP} depends dispersively on optical frequency. Middle column: characteristic isofrequency cuts through folded wavevector space at selected frequencies indicated by dashed lines, that are well below, just below, and just above the 2nd order SPP Bragg diffraction condition. Right column: characteristic radiation patterns from COMSOL corresponding to the characteristic cuts of the dispersion relation.

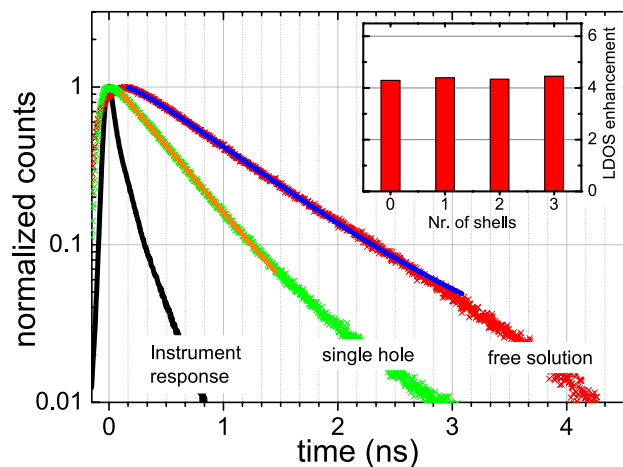
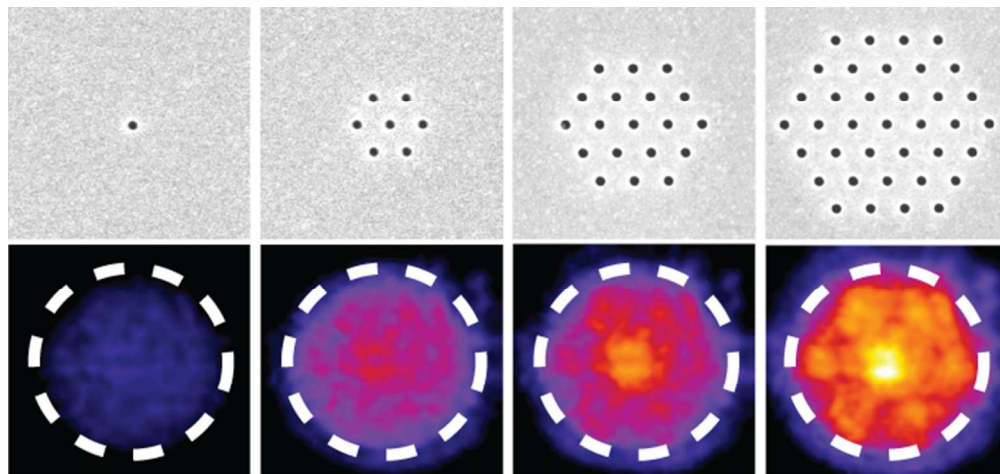


Figure 6: Normalized fluorescence decay traces for the reference solution (red markers) and the single aperture (green markers). The normalized decay traces for the hexagonal lattices with increasing number of apertures are found identical to the single aperture case. Solid lines are fitted decay curves, the black line represents the instrument response function. The insert shows the LDOS enhancement *versus* structure size.

This material is available free of charge via the Internet at <http://pubs.acs.org/>.

1
2
3
4
5
6
7
8
9
10
11
12
13
14
15
16
17
18
19
20
21
22
23
24
25
26
27
28
29
30
31
32
33
34
35
36
37
38
39
40
41
42
43
44
45
46
47
48
49
50
51
52
53
54
55
56
57
58
59
60



60x28mm (300 x 300 DPI)